Earth and Planetary Science Letters 272 (2008) 339–352

Contents lists available at ScienceDirect

Earth and Planetary Science Letters

journal homepage: www.elsevier.com/locate/epsl

Evolution of a magma-driven earthquake swarm and triggering of the nearby Oldoinyo Lengai eruption, as resolved by InSAR, ground observations and elastic modeling, East African Rift, 2007

G. Baer [a,*], Y. Hamiel [a], G. Shamir [a], R. Nof [a,b]

[a] Geological Survey of Israel, 30 Malkhe Yisrael, Jerusalem 95501, Israel
[b] Department of Geological and Environmental Sciences, Ben Gurion University of the Negev, Be'er Sheva 84105, Israel

ARTICLE INFO

Article history:
Received 20 December 2007
Received in revised form 27 April 2008
Accepted 30 April 2008
Available online 17 May 2008

Editor: C.P. Jaupart

Keywords:
earthquake swarm
volcanic eruption
dike intrusion
stress triggering
East African Rift
InSAR

ABSTRACT

An earthquake swarm struck the North Tanzania Divergence, East African Rift over a 2 month period between July and September 2007. It produced approximately 70 M>4 earthquakes (peak magnitude Mw 5.9), and extensive surface deformation, concurrent with eruptions at the nearby Oldoinyo Lengai volcano. The spatial and temporal evolution of the entire deformation event was resolved by Interferometric Synthetic Aperture Radar (InSAR) observations, owing to a particularly favorable acquisition programming of the Envisat and ALOS satellites, and was verified by detailed ground observations. Elastic modeling based on the InSAR measurements clearly distinguishes between normal faulting, which dominated during the first week of the event, and intermittent episodes of dike propagation, oblique dike opening and dike-induced faulting during the following month. A gradual decline in the intensity of deformation occurred over the final weeks. Our observations and modeling suggest that the sequence of events was initiated by pressurization of a deep-seated magma chamber below Oldoinyo Lengai which opened the way to lateral dike injection, and dike-induced faulting and seismicity. As dike intrusion terminated, silicate magma ascended the volcano conduit, reacted with the carbonatitic magma, and set off a major episode of explosive ash eruptions producing mixed silicate-carbonatitic ejecta. The rise of the silicate magma within the volcano conduit is attributed to bubble growth and buoyancy increase in the magma chamber either due to a temporary pressure drop after the termination of the diking event, or due to the dynamic effects of seismic wave passage from the earthquake swarm. Similar temporal associations between earthquake swarms and major explosive ash eruptions were observed at Oldoinyo Lengai over the past half century.

1. Introduction

An earthquake swarm consists of a sequence of seismic events of comparable magnitudes, closely clustered in time and space, and lacking a single distinct mainshock (Mogi, 1963; Sykes, 1970; Hill, 1977). The duration of a swarm is commonly a few days to a few weeks, but may vary from a few hours to a few years (Benoit and McNutt, 1996; Vidale et al., 2006). Swarms are often associated with magma intrusion (e.g., Gillard et al., 1996; Aoki et al., 1999; Toda et al., 2002; Wright et al., 2006) and in places show lateral or vertical migration, following the propagation of dikes (Einarsson and Brandsdottir, 1980). The sequential nature of intrusive and seismic events in earthquake swarms suggests that induced stress changes play an important role in their progressive deformation (Ukawa and Tsukahara, 1996; Aoki et al., 1999; Toda et al., 2002). In active rift zones, earthquake swarms are associated with surface fault scarps and extensional cracks (Pollard et al., 1983; Rubin and Pollard, 1988). However, seldom is there sufficient evidence to relate the surface deformation to specific seismic events or intrusive bodies. Previous studies that combined precise earthquake location with GPS data (e.g. Aoki et al., 1999; Toda et al., 2002) were generally successful in resolving the temporal evolution of seismicity and deformation but lacked constraints on the number, location or geometry of the faults and dikes. On the other hand, previous InSAR-based analyses of earthquake swarms (e.g., Lu et al., 2000; Lundgren and Stramondo, 2002) were more successful at determining fault locations but less successful at resolving the temporal evolution, due to insufficient SAR acquisitions during the relatively short swarm episode. In the study presented here, we resolve the full spatial and temporal evolution of faulting, magma intrusion and surface deformation associated with an earthquake swarm that struck the north Tanzania sector of the East African Rift on July 2007, by integrating seismic data, exceptionally frequent InSAR measurements, elastic modeling and detailed ground observations.

Many earthquake swarms have been temporally associated with eruptions at nearby volcanoes (Sykes, 1970; Benoit and McNutt, 1996; Linde and Sacks, 1998). These swarms may occur before, during or after

* Corresponding author.
E-mail address: baer@gsi.gov.il (G. Baer).

0012-821X/$ – see front matter © 2008 Elsevier B.V. All rights reserved.
doi:10.1016/j.epsl.2008.04.052

the initial eruption, possibly suggesting mutual triggering relationships (Nakamura, 1975; Hill et al., 2002; Walter and Amelung, 2006). Volcanic eruptions may be triggered by earthquake-induced static stress changes which can either increase the pressure in the magma chamber or unclamp the surrounding fracture system (e.g., Walter, 2007). Alternatively, dynamic stress changes generated by earthquakes may also trigger eruptions at nearby or remote volcanoes (Manga and Brodsky, 2006, and references therein). In the final part of this paper we discuss such association of north Tanzanian earthquake swarms with eruptions of the Oldoinyo Lengai volcano in 2007 and over the preceding half-century.

2. Geological, volcanological and seismological background

The East African rift (EAR), a ~5000 km-long complex boundary between the Nubian and Somalian tectonic plates, extends from the Afar depression in the north to Mozambique in the south (McKenzie et al., 1970; Jestin et al., 1994). In the Lake Natron region, northern Tanzania, the eastern branch of the EAR diverges from a single, ~50 km wide and well defined N–S trending rift in Kenya, to a 200–300 km wide extension zone in Tanzania and terminates southward (Fig. 1). Here, the distinct Pangani, Manyara and Eyasi rifts, trending NW, N–S, and NNE respectively, form an apparent "triple junction" geometry (Baker et al., 1972; Dawson, 1992; Foster et al., 1997). This "North Tanzania Divergence" (NTD) (Baker et al., 1972) has been noted for its relatively high level of seismicity (Fairhead and Girdler, 1971), a deep upper mantle thermal anomaly (Nyblade et al., 2000), and the world's youngest and only active carbonatitic volcano, the Oldoinyo ("Mountain" in Massai) Lengai ("God", "Rain" or "Snow").

Based on the geological relations between the volcanic rocks and the rift structures, the major rifting phase, which produced the present-day escarpments in this area, took place between 1.15 and 1.2 Ma (MacIntyre et al., 1974). Due to the poor accessibility of this region and the small number of permanent GPS stations, little is currently known about the relative motion between the Nubian and Somalian plates. Calais et al. (2006), suggest the existence of a counterclockwise rotating Victoria microplate consisting mainly of the Tanzania Craton between the eastern and western branches of the EAR. The relative opening rate across the EAR at this latitude was estimated to 2–4 mm/yr (e.g., Stamps et al., 2008). To resolve the regional motions, a GPS campaign was carried out in northern Tanzania in August 2006, however, results of repeat measurements after the year 2007 are not available yet.

Volcanic activity along the EAR dates back to Eocene–Oligocene times with trap basalts on the plateaus and rift margins. In the NTD zone, volcanism commenced at the early Pliocene (ca. 5 Ma) (Foster et al., 1997) and continues in the present. Eruptions of Oldoinyo Lengai initiated <0.37 Ma ago with nephelinitic and phonolitic tuffs and agglomerates (MacIntyre et al., 1974; Dawson et al., 1995). The earliest observation of natrocarbonatites was dated at about 1250 years ago (Dawson, 1993). Scientific accounts of the volcano commenced at the beginning of the 20th century. Since then, the volcano has erupted natrocarbonatitic lava periodically, with alternating periods of lava effusion, typically preceding shorter periods of ash eruptions and periods of repose (e.g., Dawson et al., 1995). The origin of carbonatitic lavas has been under debate and problematic since their discovery (Dawson, 1962). Recent studies suggest that they form by liquid immiscibility at low pressures and low temperatures and exsolution of

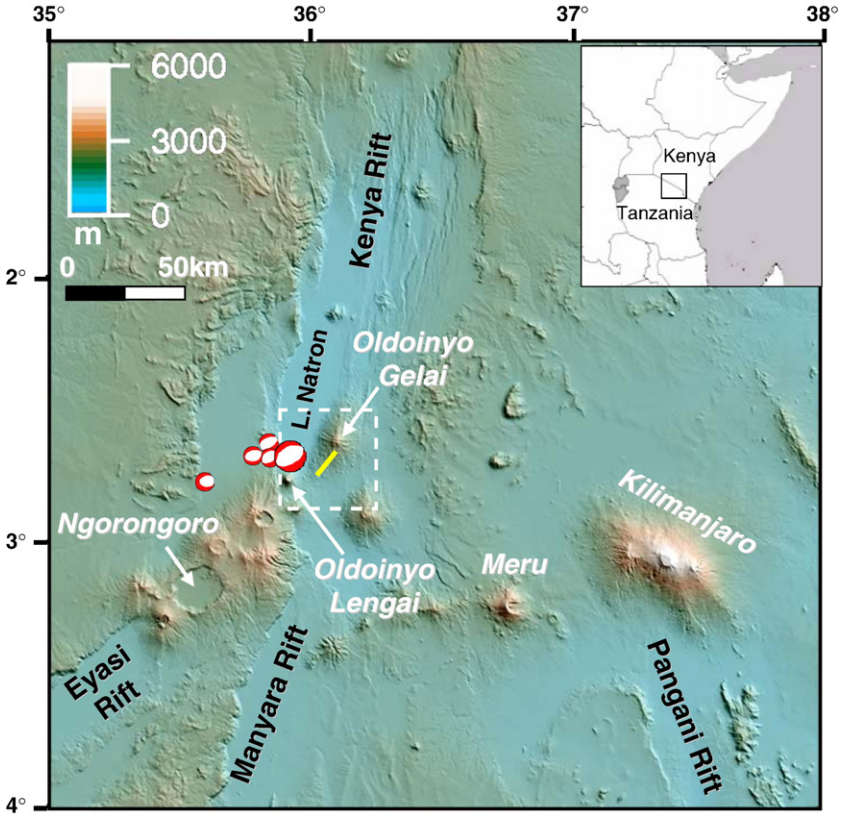

Fig. 1. Location map for the 2007 Oldoinyo Gelai earthquake swarm in the "North Tanzania Divergence", where the Kenya Rift splits southward to form the Eyasi, Manyara, and Pangani Rifts. White rectangle marks the swarm area, shown in detail in Figs. 3, 4 and 6. Red beach-ball symbols shows the global CMT locations and focal mechanisms of the first M>5 earthquakes (The peak Mw 5.9 earthquake of July 17, 2007 is marked by a larger symbol). Yellow line marks the location of the main rupture surface associated with the peak event as observed by InSAR and verified by ground observations (see Sections 4 and 5 below). (For interpretation of the references to color in this figure legend, the reader is referred to the web version of this article.)

an alkali-rich carbonate liquid from a highly evolved, CO_2-rich wollastonite nephelinite magma (e.g., Peterson and Kjarsgaard, 1995).

An intriguing correlation emerges by comparing the earthquakes record (catalogue of the International Seismological Center, 2001) with that of the volcano activity, in particular for major ash eruptions. Fig. 2 summarizes this comparison in a 2° by 2° area centered at the volcano for the years 1960–2008. The violent explosion in August 1966, at the end of a six-year period of silent lava extrusion, was preceded by a swarm of ten M_b>3.4 (peak magnitude 4.1) earthquakes in the nearby region (Fig. 2b). Similarly, the major explosive event of July 1967, which emitted ash as far as Arusha and Nairobi, followed three M_b>4.2 earthquakes in the preceding week (Fig. 2b), and the ash eruption that began on June 14, 1993 was preceded by an M 5.3 earthquake on April 11 and another earthquake on June 14 (Fig. 2c) (Dawson et al., 1995). It should be noted, however, that not all recorded earthquake swarms have been correlated with specific eruptions. The silent carbonatitic lava effusion events are uncorrelated with specific earthquakes or swarms (Fig. 2). In addition, the low accuracy of reported epicenter locations (particularly for earlier times) limits our ability to distinguish between nearby and remote swarms within the examined area. During the 1966 and 1993 eruptions unusual mixtures of carbonate and silicate materials were found in the emitted ash (Dawson et al., 1992, 1994), in contrast with the domination of carbonatites in all other eruptions during the last 50 years.

3. The 2007 earthquake swarm and associated volcanic activity

Starting on July 12 and continuing until mid September, 2007, an earthquake swarm struck the Oldoinyo Gelai region (Fig. 1), producing about seventy M>4 earthquakes. Initial determination by global

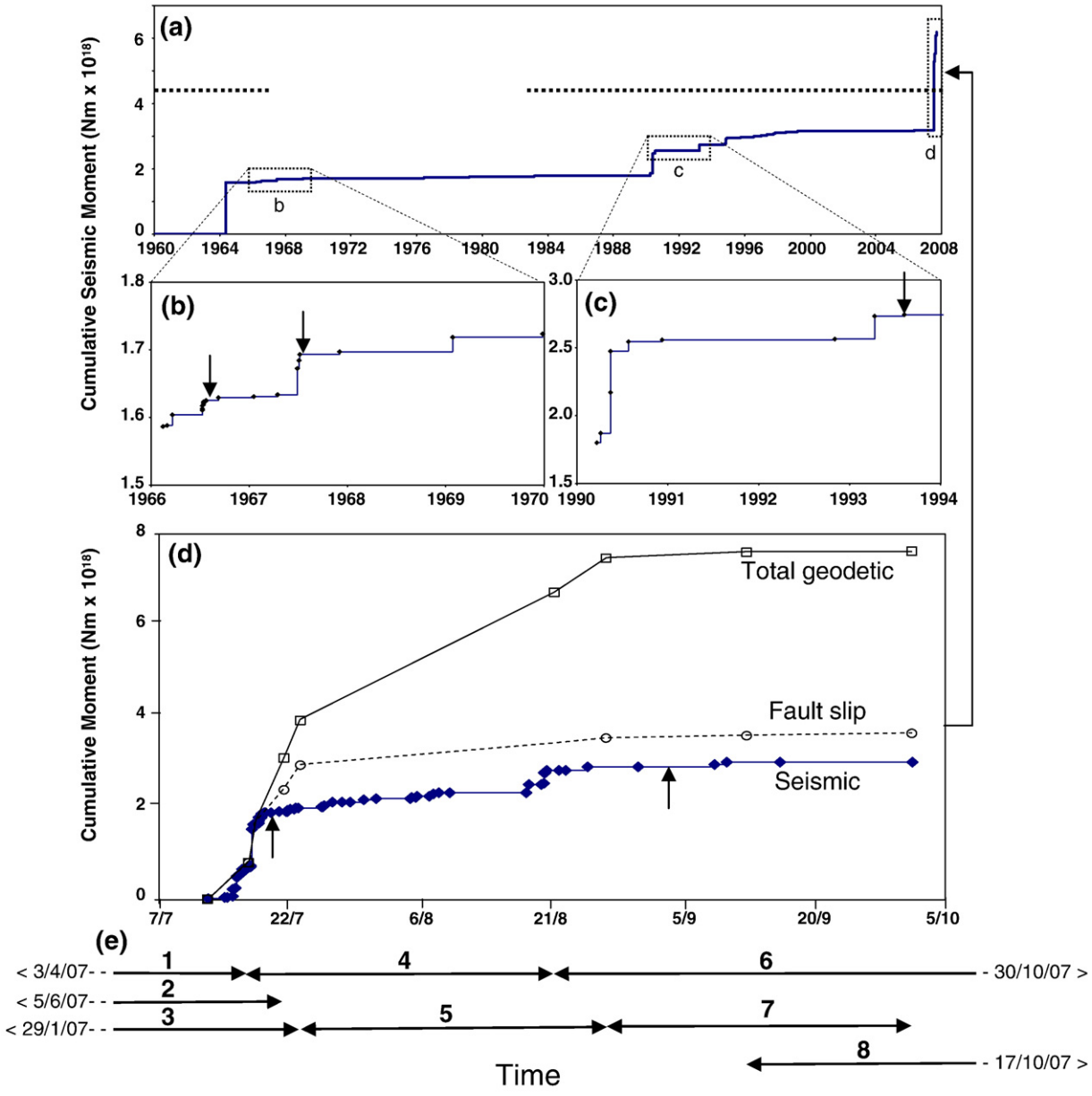

Fig. 2. Cumulative seismic moment release in the rectangle S2 °–S4 °, E35 °–E37 °, calculated using empirical global relations between body-wave magnitude (M_b), moment magnitude (M_w), and seismic moment (M_o) (Kanamori, 1977; Scordilis, 2006). Major ash eruptions and lava effusion periods of Oldoinyo Lengai volcano are marked by vertical arrows and thick horizontal dashed lines, respectively. (a) Overall accumulation in the period 1960–2008; (b) Details of the 1966–1967 period. (c) Details of the 1993 period. (d) Cumulative seismic moment, cumulative fault-slip geodetic moment, and cumulative total (fault-slip + opening) moment released during the 2007 episode (based on the InSAR modeling below). The left vertical arrow marks the onset of the 2007 effusive eruption and the right arrow marks the onset of the major ash eruption of Oldoinyo Lengai. (e) Interferometric pairs used in this study, marked by horizontal arrows, and numbered as in Fig. 3 and Table 1.

broadband networks (NEIC and EMSC catalogs) showed epicenter distribution over an area about 50×50 km wide. Global Centroid Moment Tensor solutions (CMT) for the first five M>5 events (including the peak event) show normal faulting on ENE to NE striking focal planes in the near vicinity of Oldoinyo Lengai (Fig. 1). A regional seismological experiment was launched in June 2007 in the region surrounding the North Tanzania Divergence (Richard Wambura-Ferdinand, personal communication, 2007), however, results of that experiment are yet unpublished.

Effusive eruptions began at Lengai on July 19, 2007, 2 days after the peak M_w 5.9 event. On 3–4 September 2007, a major ash eruption began, covering areas as far as 20 km away from the volcano. This phase of ash eruption, occasionally very violent, has intermittently continued into April 2008. Samples from the 24th September 2007 ash eruption show that the volcano produced a hybrid magma formed by the interaction between natrocarbonatite and nephelinite, which seems to be similar in some ways to the 1966 ash (Mitchell and Dawson, 2007).

4. InSAR processing and modeling

4.1. Methods and results

Over the last two decades, Interferometric Synthetic Aperture Radar (InSAR) has become a widespread tool to measure subtle displacements at the ground surface (e.g., Massonnet and Feigl, 1998). Given the absence of repeat GPS data in the Mt. Gelai area after the 2007 earthquake swarm, InSAR observations provide the only non-seismological constraints on the source parameters of the 2007 earthquakes. We used ASAR images from the European Space Agency

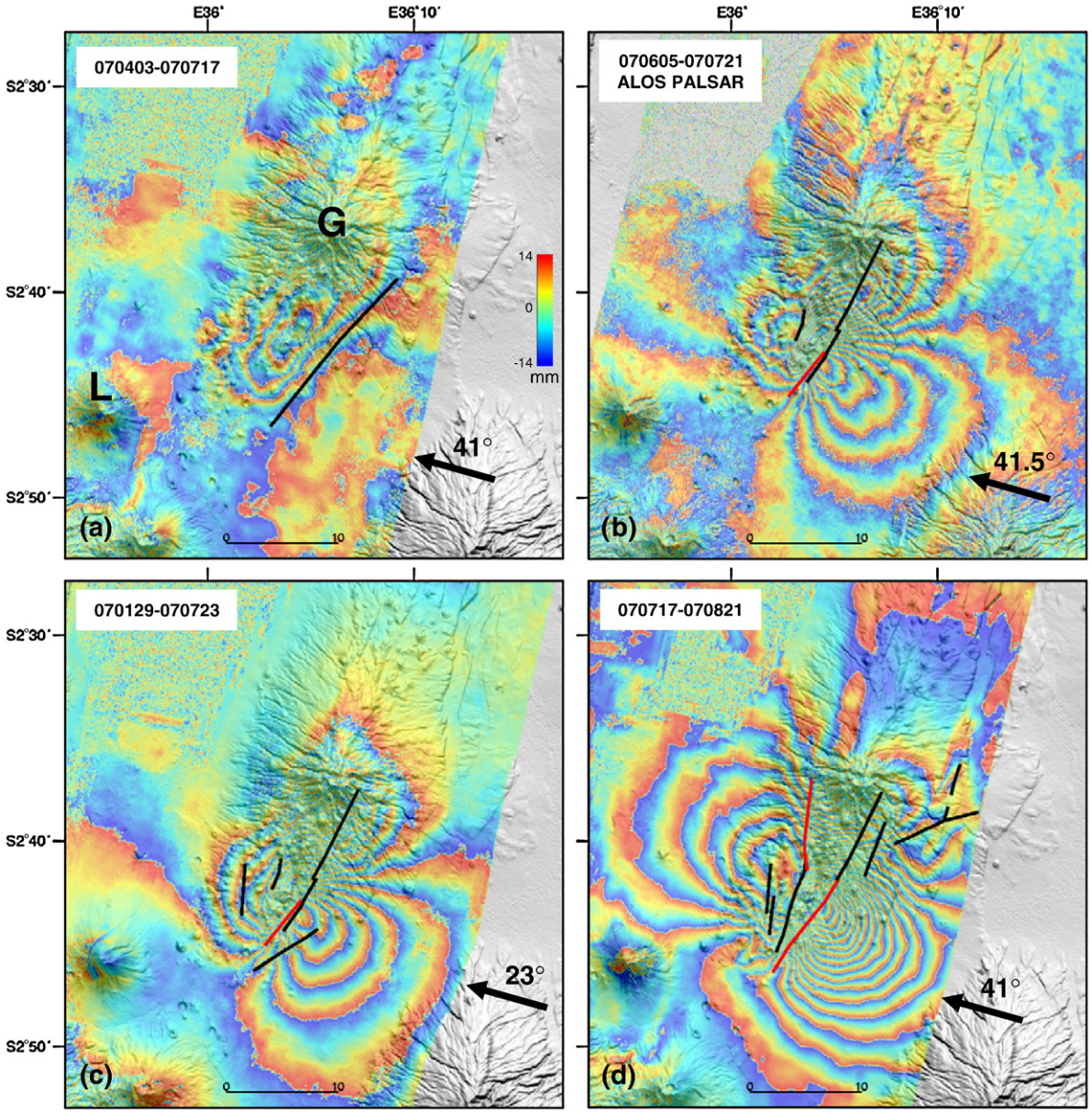

Fig. 3. Interferograms calculated in this study, draped over an SRTM Digital Elevation Model. All interferograms are produced from Envisat ASAR images, except when differently stated. Each fringe cycle corresponds to 28 mm displacement in the satellite to ground direction. Arrows mark the look directions, with incident angles shown above. The inferred fault ruptures are marked by black lines and the inferred dikes are marked by red lines. G – Oldoinyo Gelai; L – Oldoinyo Lengai. Note that the interferogram spanning the interval between September 12 and October 17 shows deformation that is also evident in the previous interferogram, indicating that surface deformation diminished between September 12 and October 1. (For interpretation of the references to color in this figure legend, the reader is referred to the web version of this article.)

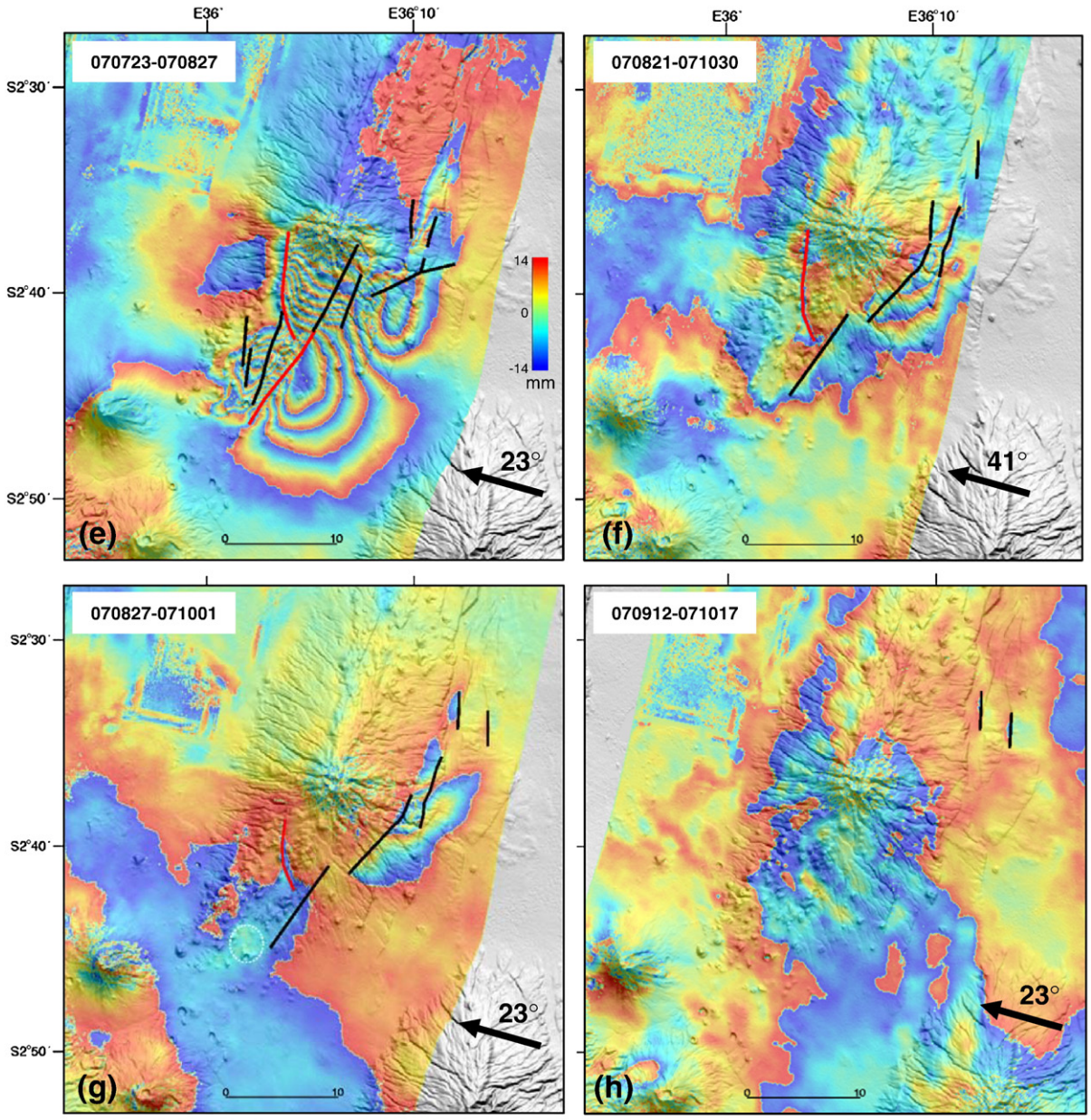

Fig.3 (*continued*).

(ESA) ENVISAT satellite and PALSAR images from the Japan Aerospace Exploration Agency (JAXA) ALOS satellite. The ASAR data (C-band, 5.6 cm wavelength) were acquired in beam modes IS2 and IS6 (mean incidence angles of 23° and 41°, respectively), and were processed using the JPL/Caltech ROI-PAC software (Rosen et al., 2004). The PALSAR L-band data (23.6 cm wavelength, mean incidence angle of 41.5°) were processed using the GAMMA software (Werner et al., 2003). We remove the topographic phase from the phase changes due to ground displacements and geocode the interferograms using NASA's 3 arc second Shuttle Radar Topographic Mission (SRTM) digital elevation model (DEM) (Farr and Kobrick, 2000; Jarvis et al., 2006).

Eight interferometric pairs, in partly-overlapping intervals, captured the surface deformation associated with the earthquake swarm in Mt. Gelai, (Figs. 2e, 3). Deformation fields are represented by interference (phase change) fringes (Fig. 3), each fringe cycle corresponding to 28 mm of movement along the satellite line-of-sight (LOS) direction. Because of the relatively short temporal and spatial baselines between the orbits (Table 1), most interferograms allow nearly complete spatial coverage of the phase changes. The ALOS interferogram of the period spanning the peak event (Figs. 2e, 3) is fully coherent in the region of maximum

Table 1
Interferometric pairs used in this study (Figs. 2e, 3)

#	Satellite	Dates (yymmdd)	Track	Inc (°)	Time (days)	Baseline (m)
1	ENVISAT	070403–070717	6	41	105	145
2	ALOS	070605–070721	236	41.5	44	514
3	ENVISAT	070129–070723	92	23	175	22
4	ENVISAT	070717–070821	6	41	35	42
5	ENVISAT	070723–070827	92	23	35	6
6	ENVISAT	070821–071030	6	41	70	84
7	ENVISAT	070827–071001	92	23	35	30
8	ENVISAT	070912–071017	321	23	35	47

deformation (unlike the corresponding ENVISAT interferograms) (Fig. 3), and adds an important time partition 4 days after the peak event. In each interferogram the traces of surface ruptures are inferred from phase discontinuities (Fig. 3), which are usually restricted to specific interferograms. However, in several locations they persist through sequential interferograms (for example, the southern dike segment shown in Fig. 3b, c, d, and e), indicating ongoing deformation, rather than short-term seismically-induced events.

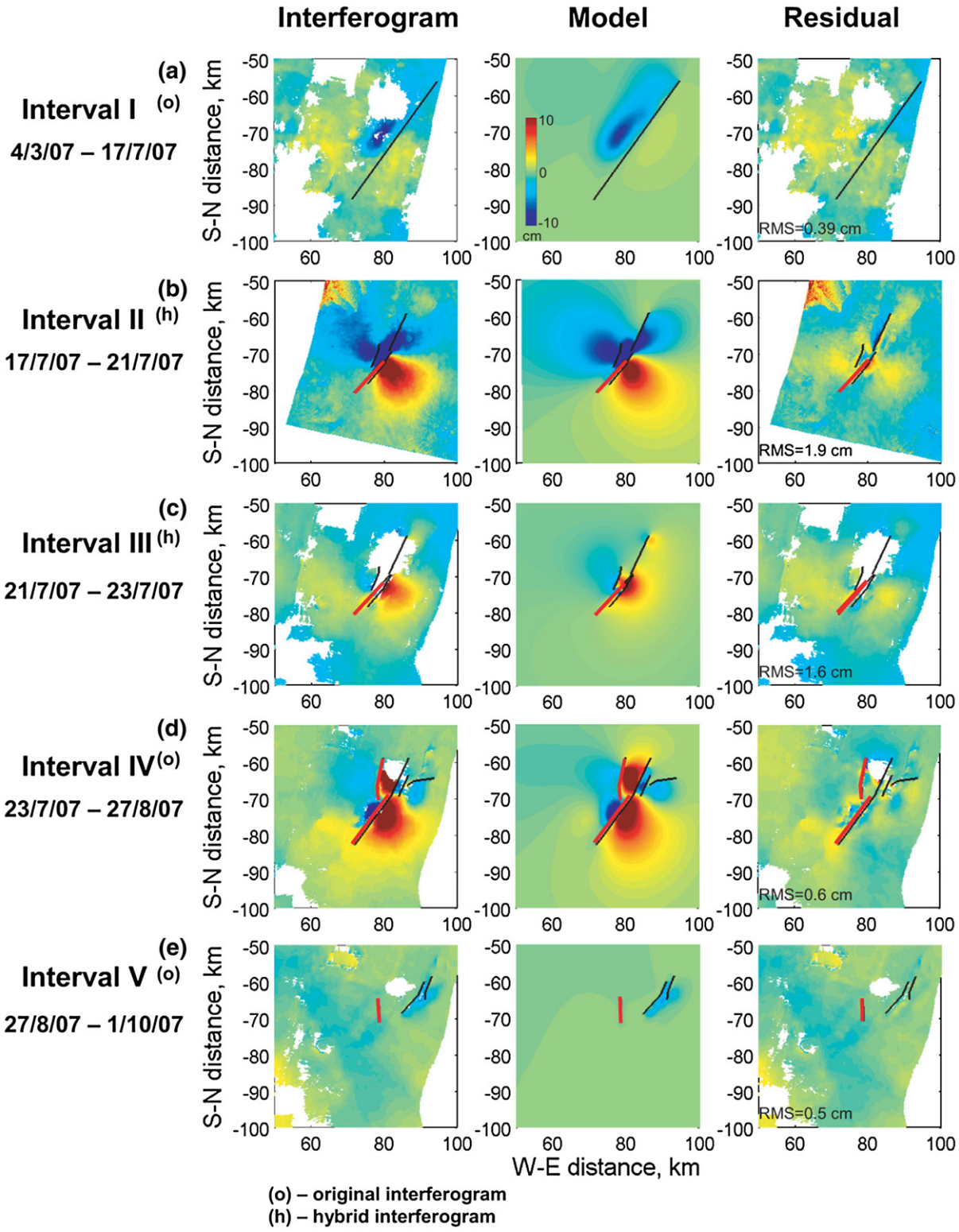

Fig. 4. Left: Original and "hybrid" unwrapped interferograms used for the inversion (local UTM coordinates, origin at 35.358 °E, 2.059 °S). Fault and dike traces, marked by black and red lines, respectively, follow discontinuities in the wrapped interferograms (Fig. 3). Center: Model (synthetic) interferograms obtained by inversion of the corresponding data interferograms. Right: Residuals between interferograms and models. Positive values (red) mark movement towards the satellite. (For interpretation of the references to color in this figure legend, the reader is referred to the web version of this article.)

4.2. Inversion of InSAR measurements

InSAR observations are often interpreted by simple models based on solutions for the elastic fields produced by rectangular dislocation planes in an elastic half-space (Okada, 1985). An inversion scheme (e.g., Fialko, 2004; Hamiel and Fialko, 2007) is applied, based on a least squares minimization of the displacement misfit with iterations for the fault geometry. The inversion scheme includes sub-sampling of the SAR data using a recursive quad-tree algorithm (e.g., Jónsson et al., 2002). Throughout the interferogram the data are sub-sampled on a homogenous grid with spacing of ~5 km. Closer than ~20 km from the main faults and dikes the sampling algorithm selects additional points that are essential for high resolution description of the original data sets with a precision given by linear interpolation. In this way we account for the observed deformation pattern and avoid most of the noise. The initial fault pattern in our models was inferred from discontinuities in the wrapped InSAR data (Fig. 3), and verified by direct field inspection of the surface ruptures. To account for the non-planar geometry of the surface ruptures we initially divided the fault traces into several vertical rectangular segments. To account for the spatially variable slip distribution, each segment was further subdivided into 1×1.5 km, constant-slip patches, allowing only pure normal slip and opening modes throughout the inversion. The slip model was smoothed in order to minimize the opening and slip gradients produced by both the dikes and the faults. We also imposed positivity of the opening and normal slip. For each inversion, we chose the slip model that was the smoothest and with the lowest RMS value. As the seismic velocity structure of the crust in this region is poorly constrained, we calculated the slip distribution by assuming a homogeneous half-space model.

The altitudes of ambiguity of the interferograms used in our inversion are between 70 m and 1600 m, which are considerably higher than the ~7 m accuracy of the SRTM DEM used to correct the topographic phase. We thus presume that the major source of noise in the data is not DEM errors but atmospheric conditions that delay the radar signal differently at each acquisition time. We distinguish

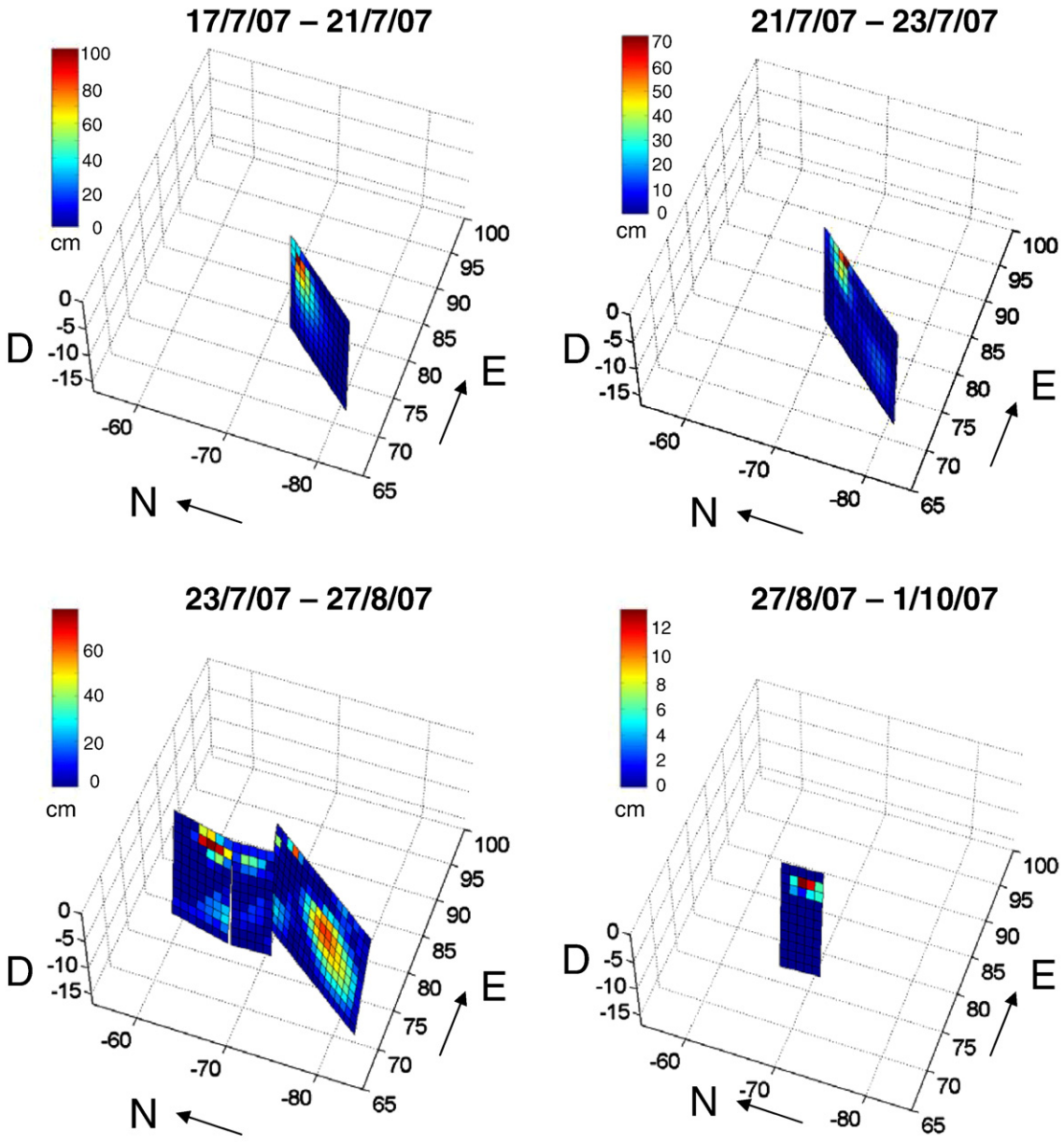

Fig. 5. Best-fit dike-opening models obtained by inversion of the InSAR measurements for 4 consecutive time intervals. Depth (D), East (E) and North (N) units are in km.

between an irregular pattern resulting from turbulent processes in the atmosphere and a signal resulting from vertical stratification and different vertical refractivity profiles during the two SAR acquisitions. The atmospheric effects are naturally more pronounced when the deformation signal is lower, as is the case in the late interferograms (Fig. 3f–h). However, in these latter interferograms we do not see any topographic-correlated signal around the Lengai and Gelai mountains, and we thus neglect these possible effects in our inversions.

Because the overlapping pairs of interferograms were acquired at different view angles, along different tracks and, in one case, by a different satellite (Fig. 2e), simple interferogram subtraction does not provide the net deformation for the non-overlapping intervals. Thus, in order to resolve the chronological order of events, we created new "hybrid" interferograms in the following way. First, we inverted the deformation measurements of one interferogram in an overlapping pair and generated a fault slip model. Then we projected the model into the line of sight of the second interferogram, and finally, we subtracted the model from the second interferogram. It should be noted that errors incorporated into the models may propagate through the time series (see discussion below). This procedure provided a sequence of interferograms for the entire swarm period, spanning all the intervals between the SAR acquisition dates. The shortest such interval was 2 days long (Fig. 2e).

Based on the availability of the original interferograms and the new "hybrid" interferograms created by the procedure described above, we inverted the deformation for five major InSAR intervals. Our best-fit inverted models explain 87%–99% of the observed deformation with respective RMS values between 1.9 cm and 0.3 cm (Fig. 4; Table S1). The higher RMS values were found in models derived from inversions of the "hybrid" interferograms. Surface deformation during most of the swarm period can only be explained by both fault slip and dike opening, occurring either on single or on separate structures. The model results for the five InSAR intervals (I–V) are shown in Figs. 4, 5, S1 and in Table S1. The temporal evolution of events is resolved as follows:

InSAR interval I, preceding the July 17 peak event: The model indicates dip-slip displacement on a blind fault dipping 40° to the northwest with maximum slip of about 30 cm at 5–7 km depth.

InSAR interval II, July 17–21: Deformation migrated to the northwest. The inverted model indicates: (1) Dip-slip on a fault segment dipping 50° to the northwest, corresponding to the peak M_w 5.9 event, (2) Dip-slip on sub-parallel faults, (3) up to 1 m opening at ~2 km depth across a vertical dike situated a few hundred meters west of the main fault.

InSAR interval III, July 21–23: upward migration of the slip and opening patches along the July 17–21 major fault and dike, respectively.

InSAR interval IV, July 23–August 27: Southward in-plane dike propagation and opening of a step-over segment to the northwest. During this period, dip-slip faulting occurred mostly along and beyond the main opening patches, and to some extent, along minor faults east and west of the dikes. The maximum values of dip-slip and opening during that period were 120 cm and 70 cm, respectively.

InSAR interval V, August 27–October 1: About 15 cm opening of the NW dike segment below a depth of 1–3 km, and normal faulting along new ruptures to the NE of the main one, with maximum slip of about 20 cm.

Fig. 6 summarizes the spatial and temporal evolution of dikes and faults during the swarm period. Overall, the modeled fractures have a

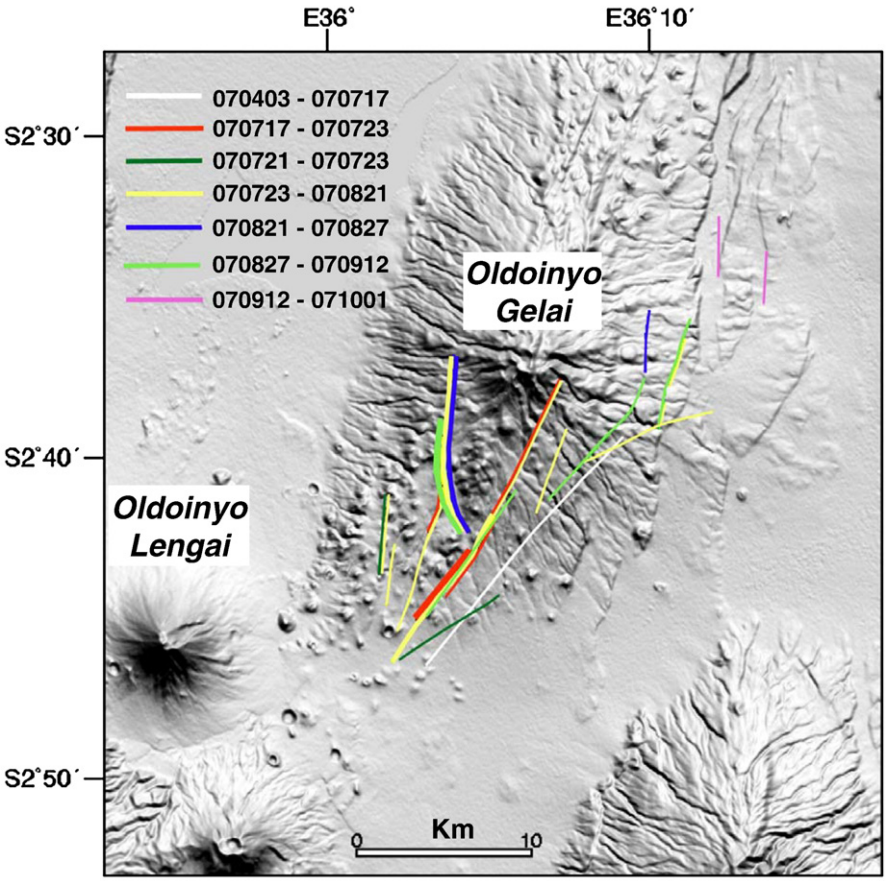

Fig. 6. Summary map of all faulting and dike intrusion events during the 2007 Gelai earthquake swarm as derived from the data and the model interferograms (Figs. 3, 4) on an SRTM DEM background, with colors representing their temporal sequence. Surface traces of faults and dikes are marked by thin and thick lines, respectively. (For interpretation of the references to color in this figure legend, the reader is referred to the web version of this article.)

northeastward radiating pattern, with activity migrating in time in the same direction. An LOS increase, interpreted as subsidence is observed during the final stages of deformation close to the fracture convergence area (Fig. 3g). These observations may suggest the existence of a magma source near the fracture convergence area, and propagation of dikes and faults along stress trajectories. It is further observed (and confirmed by ground observations) that several new fractures followed traces of existing faults expressed in the DEM.

5. Ground observations

Immediately following the earthquake swarm, we carried out a field survey at the southern flanks of Oldoinyo Gelai, in order to obtain temporal and spatial constraints on the surface deformation, before surface ruptures erode. The majority of InSAR-inferred ruptures were accurately verified in the field, showing a few to several tens of centimeters of vertical and/or opening offsets on fresh soil and rock scarps. Along the rupture trace of the peak event, vertical offset reached 50 cm (Fig. 7a) and sub- parallel cracks formed graben structures, several meters wide (Fig. 7b). The average spacing between major faults is about 2 km (Fig. 6). A ~400 m wide shallow graben formed between the main fault and a parallel rupture to the northwest (Fig. 7c). This graben follows the estimated trace of the modeled dike. Smaller rupture surfaces found in the field are attributed to other M>5.0 earthquakes. These faults show up to 20 cm of both dip-slip and opening displacements along en-echelon segments (Fig. 7c) that indicate, in places, minor left-lateral slip components. Independent information concerning the sequence of events was provided by the local inhabitants, as follows: after the peak earthquake occurred on July 17, minor parallel cracks with vertical offsets of a few cm appeared. Then, over the following few weeks, gradual subsidence occurred along a narrow NE-striking zone parallel to the major rupture, and minor cracks appeared in several additional locations. We interpret this gradual subsidence as a response to continuous subsurface extension, consistent with our InSAR-derived models that suggested subsurface dike emplacement. After the termination of the earthquake swarm, two distinct plumes of ash, one black and one light grey were observed above Oldoinyo Lengai, at some occasions simultaneously (Fig. 7d).

6. Discussion

Our observations show a sequential order of seismic, intrusive and eruptive events in two adjacent regions. In the following discussion we explore the possible mechanisms for this temporal and spatial association. We first analyze the evolution of the Gelai earthquake swarm by calculating the stresses induced from one deformation stage onto the structures involved in the next, and then discuss the possible relationships between the earthquake swarm and the violent eruptions.

6.1. Evolution of deformation

The estimated seismic moment released during the entire swarm period was $\sim 3\times10^{18}$ Nm (Fig. 2d), calculated using empirical global relations between body-wave magnitude (M_b), moment magnitude (M_w), and seismic moment (M_o) (Kanamori, 1977; Scordilis, 2006).

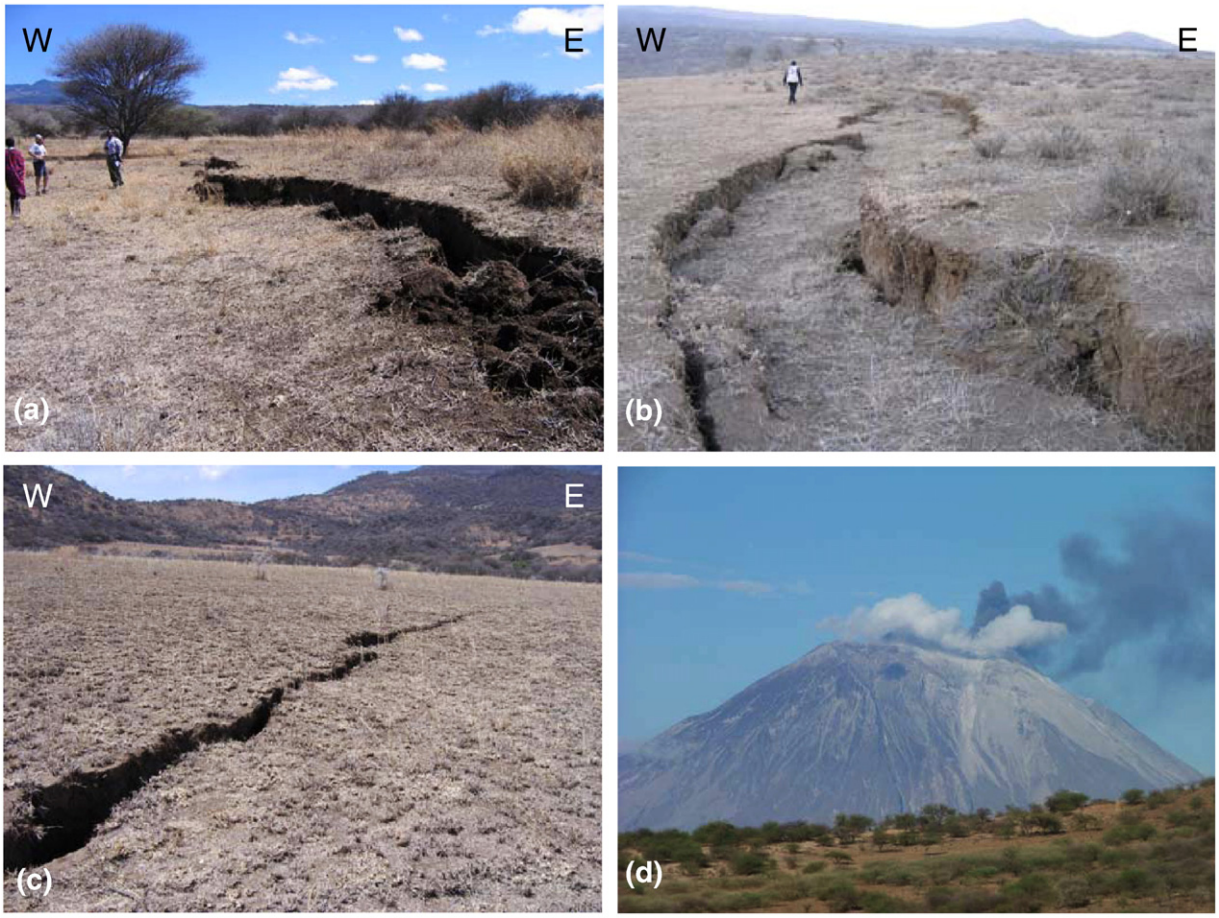

Fig. 7. (a) Fault escarpment produced by the peak Mw 5.9 event, viewed from south. (b) Small-scale graben (4–6 m wide), parallel to the main fault escarpment. (c) Northwest boundary fault of a 400 m wide graben, viewed from south, also showing left-stepping segmentation towards its northern end. (d) Concurrent emission of black and light grey ash, Oldoinyo Lengai volcano, October 19, 2007.

Calculations of the geodetic (total) moment based on the inversion models show that its total, due to both faulting and diking, was ~7.5×10^{18} Nm, of which ~3.6×10^{18} Nm was produced by faulting alone. The seismic- and fault-induced geodetic moments follow similar temporal evolution (Fig. 2d). Slightly larger geodetic values are calculated for the second and third stages, and are most likely an artifact of the poorer model-data agreement in the inversion of the "hybrid" interferograms which propagated into the next stages (Figs. 2d, 4).

The model-based temporal variation of moment release (Fig. 2d) indicates that the entire deformation event consisted of three major stages. The first took place during the first week, and was dominated by normal faulting accompanied by a large number of M>4 earthquakes. The second stage, about one month long, was dominated by intermittent lateral dike propagation, dike-opening, and dike-induced faulting episodes. Deformation gradually declined during the third stage that lasted a few weeks and terminated between September 12 and October 1 (Figs. 2–4).

Our models do not require magma intrusion before the peak event on July 17, and the surface deformation may be fully explained by normal slip on a blind fault striking 040° and inclined 40° westward, corresponding to an M_b 5.4 earthquake that occurred on July 15. However, based on later appearance of dike-induced deformation, we were motivated to check whether this early blind fault could have been associated with a rising dike when the latter was still too narrow and/or too deep to be geodetically detected by InSAR. We calculate the Coulomb stress favorable for normal slip on this blind fault, induced by a dike that is 0.2 m or 0.5 m thick (shown in vertical cross sections in Fig. 8a and b, respectively) and which produces vertical surface displacement lower than the InSAR detection limit of 5 mm (shown in

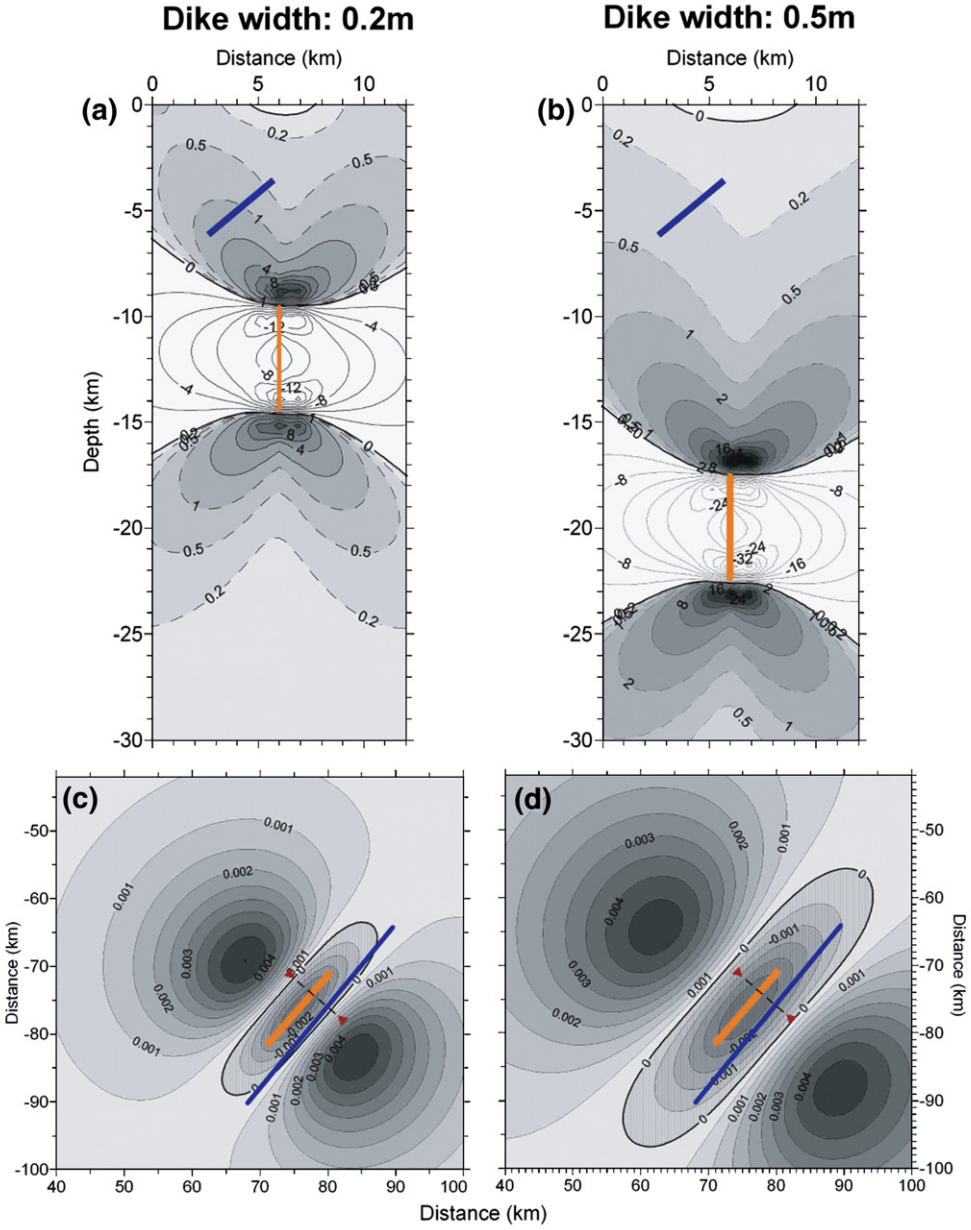

Fig. 8. (a, b) Coulomb stress change (bars) favorable for slip on the blind normal fault of InSAR interval I (strike 040°, dip 40°; blue line), induced by a deep-seated dike, 0.2 m and 0.5 m thick, shown in vertical cross sections perpendicular to the trace of the fault. (c, d) Surface vertical displacement (meters) due to each of these model dikes (respectively), showing the projected surface traces of the dike (orange), the blind fault (blue) and the cross section (broken lines). (For interpretation of the references to color in this figure legend, the reader is referred to the web version of this article.)

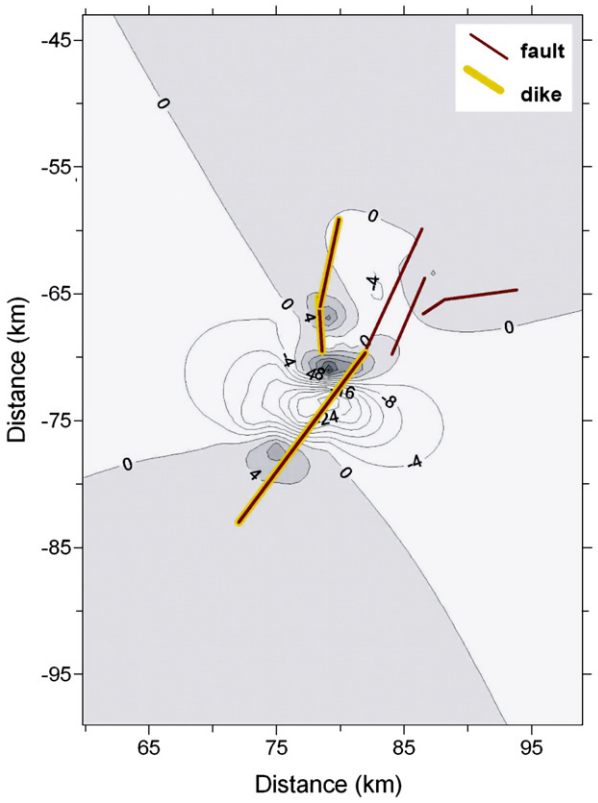

Fig. 9. Map view distribution of E–W normal stress (bars; tension positive) at 5 km depth, produced by the dike and faults active during InSAR interval II (July 17–21), overlain by the surface traces of dikes and faults of interval IV (July 23 to August 27). Note that these dikes and faults formed where the induced tensional stress of the earlier interval was greatest.

map view in Fig. 8c and d, respectively). The calculation utilizes an implementation of 3D elastic dislocation solutions in a boundary elements numerical model (Toda and Stein, 2002), with a shear modulus of 30 GPa, Poisson ratio of 0.25 and effective friction coefficient of 0.4. In these model dikes, the induced Coulomb stress favorable for normal faulting (positive) on the modeled blind fault is in the range 0.1–1.5 bar. These results show that blind faulting in Stage I may well have been induced by a dike at a depth on the order of 10 km and several tens of centimeters thick, which was undetected at the surface.

The second deformation stage was dominated by intermittent dike propagation and dike-induced faulting episodes. Faults formed mainly parallel to and along the continuations of propagating dike segments. The role of static stress transfer in the evolution of this seismic-intrusive process can be evaluated by calculating the horizontal normal stress produced at various stages. For example, faulting and dike opening during InSAR interval II (Fig. 4) produced a tensile E–W normal stress distribution which apparently determined the penetration pattern of the step-over dike to the northwest during InSAR interval IV (Fig. 9). For this calculation, fault and dike discretization and static source parameters (geometry, slip distribution) are based on the InSAR inversion models, with elastic parameters as above.

6.2. Earthquake–volcano interaction

Since the earthquake swarm in Gelai was to a great extent induced by dikes, the question of whether the dikes and the Lengai volcanic eruptions originated from a common magma source is important for understanding the earthquake–volcano interaction. The Gelai dike and fault traces converge southward to a point that is about 10 km east of the Lengai volcano. It is thus reasonable to assume that the approximate margin of the Lengai magma source is located at depth of several km under this point. This is also consistent with the temporal migration direction of faulting and dike intrusion from southwest to northeast. We thus suggest that the dikes originated from a deep-seated magma chamber underlying Lengai, and propagated away first laterally and then vertically.

An additional noteworthy observation is the temporal relations between the dike intrusion and the explosive Lengai eruptions (Fig. 10). Our InSAR modeling show that the major period of dike intrusion at Gelai was between July 17 and August 27, 2007, with minor (~15 cm) opening between August 27 and September 12. The major ash eruption at Lengai initiated on September 3–4, just as the major stage of dike intrusion ended.

The magma system at Oldoinyo Lengai was previously described as a density- and immiscibility-stratified chamber with natrocarbonatitic magma overlying alkali-silicate magma (Kjarsgaard and Hamilton, 1989). The sub-volcanic structure of Oldoinyo Lengai has been modeled as a two-level magma chamber (Petibon et al., 1998), the deeper at ~100 MPa (~3.3 km depth), and the shallower at ~20 MPa (~0.6 km depth). A chamber at greater depth has not been proposed, yet the occurrence of dikes as deep as 15 km (Fig. 5) suggests the existence of an additional deep-seated magma source. Explosive ash eruptions, in contrast with the silent extrusions of carbonatite lavas, were attributed to the reaction of carbonatite with pyroxene and wollastonite, which releases CO_2 (Dawson et al., 1992). The suggested mechanism for this reaction and mixing between the two phases was the gradual evacuation of the upper carbonatitic phase (as occurred between 1960 and 1966) until the pressure in the magma chamber dropped below the level required to maintain immiscibility (Dawson et al., 1992). Accepting that the major driving mechanism for the explosive eruptions in Lengai is the mixing of the two phases and bearing in mind the abovementioned temporal association of dikes and earthquake swarms with major ash eruptions, we suggest the following scenario for the Gelai-Lengai earthquake-volcano interaction.

Pressurization of a deep-seated magma source below Oldoinyo Lengai led to northeastward lateral propagation of dikes and induced seismic faulting. One week after the swarm onset, effusive natrocarbonatitic eruptions began at the volcano, possibly due to shaking effects in the upper magma chamber. Magma withdrawal by lateral dike injection away from the source during the next month caused temporary pressure decrease and increased buoyancy within the

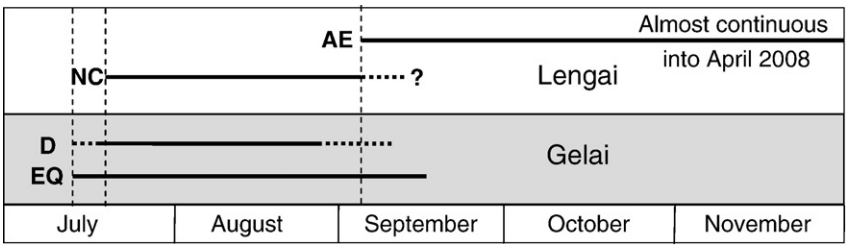

Fig. 10. Temporal relations between the 2007 earthquake swarm (EQ) in Gelai and the eruptive history at Lengai. Natrocarbonatitic (NC) effusion at Lengai started a week after the first earthquake (2 days after the peak earthquake) in Gelai, and ash eruptions (AE) began as the dike intrusion period (D) in Gelai terminated.

magma chamber, possibly due to bubble formation. With further supply of magma, this process eventually led to ascent of lighter, bubble-rich silicate magma into the volcano conduit, which reacted with the carbonatitic magma above, and set off the major episode of explosive ash eruptions and mixed silicate-carbonatitic ejecta.

6.3. Earthquake triggering

The temporal correlation between earthquake swarms and eruptions in Oldoinyo Lengai in the past half century is notable, and consists of three key observations. (1) The major violent ash eruptions occurred after earthquake swarms. (2) The 2007–2008 ash eruption was the longest and most voluminous event since 1960, and the 2007 earthquake swarm was the longest and of the highest magnitudes in this region during the instrumental era. (3) The 1966, 1993, and the 2007 eruptions emitted mixtures of carbonatites and silicates, in contrast to the dominant carbonatite magma otherwise extruded throughout the last half-century. The occurrence of dikes and earthquakes in the Lengai region may thus play a role in triggering the ash eruptions. In the following we examine the possible effects of two dominant modes of triggering.

6.3.1. Static triggering

Earthquake-induced static stress changes may trigger an eruption by increasing the mean compressive stress in the vicinity of the volcano and consequently the pressure in the magma body (e.g. Hill et al., 2002). Alternatively, a drop in the mean compressive stress could promote melting and bubble formation or unclamp fractures around the magma chamber, leading to similar results. Recent studies (e.g., Stein, 2004; Walter and Amelung, 2006; Walter, 2007) show that static stress changes in the order of 1–10 bars may promote volcanic eruptions.

We calculate the change of mean stress induced by the diking and faulting events in July and August 2007, based on the model parameters of InSAR intervals I-IV using a bulk modulus of 5.33×10^5 10^5 bars. The calculated overall stress change at depths of 5 km and 10 km under the volcano are zero to slightly positive (order of 0.01 bar; Fig. 11). Based on these low mean stress values, we conclude that it is unlikely that static stress changes associated with the 2007 Gelai deformation event played any role in triggering the Lengai eruptions.

6.3.2. Dynamic triggering

Variations in earthquake frequency and volcanic activity observed as far as 1200 km from the 1992 Landers earthquake (Hill et al., 2002) were attributed by Linde et al. (1994) to dynamic effects. They suggest that the passage of seismic waves from earthquakes may cause advective overpressure in magma bodies by detaching bubbles from the floor and walls of their chambers. The rise of such bubbles may increase magma pressure by several MPa. Bubbles may also grow and ascend due to pressure oscillations induced by passing seismic waves or due to overturn of the magma chamber by shaking (Hill et al., 2002). Depending upon the magma viscosity, the rise and growth of

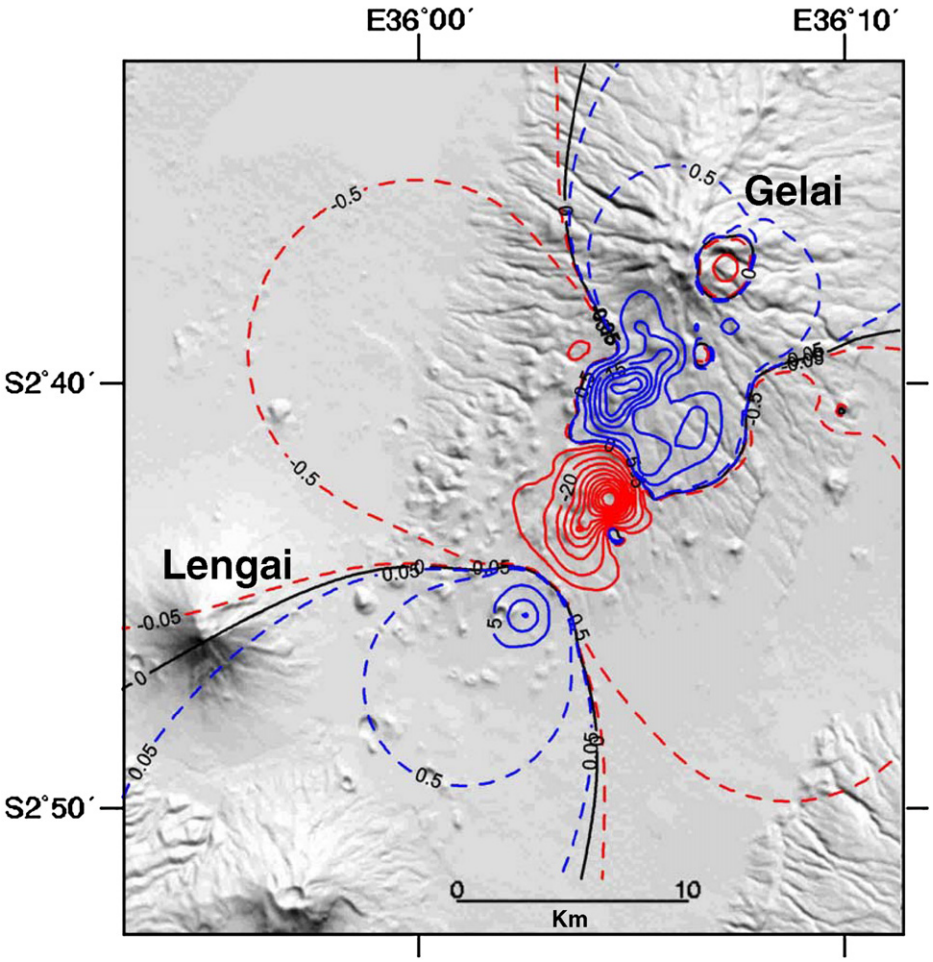

Fig. 11. Distribution of mean normal stress (positive for unclamping) induced by the diking and faulting events in July though August 2007, at a depth of 5 km below Oldoinyo Lengai. The fault parameters are based on the model inversion parameters of InSAR intervals I–IV, with a bulk modulus of 5.33×10^5 10^5 bars.

these bubbles may last a few days, which should be the delay time between the earthquakes and subsequent eruptions.

We suggest that during the Gelai earthquake swarm, the passage of seismic waves through the nearby Lengai magma chamber may have also promoted the growth and ascent of bubbles in the deep, silicate chamber. Bubble growth would increase the magma buoyancy in the chamber and lead to magma ascent. The level of shaking will strongly depend on the correlation between the frequency content of the seismic waves and the size of the magma chamber, causing either amplification or damping effects. We thus consider the dynamic effects due to the earthquake swarms as a plausible supporting trigger for the silicate magma ascent and mixing that produced the violent ash eruptions.

7. Conclusions

The combination of InSAR measurements, ground-truth verification and elastic modeling provides a detailed account of the evolution of the 2007 North Tanzania Divergence magma-driven earthquake swarm, from its onset, through an intensifying period, to its final decline. We show that the earthquake swarm and volcanic eruptions at the nearby Oldoinyo Lengai volcano were coupled. The event initiated by pressurization of a deep-seated magma chamber below Oldoinyo Lengai, followed by lateral dike injection and dike-induced faulting in the Mt. Gelai area. Explosive ash eruptions producing mixed silicate-carbonatitic ejecta followed the termination of dike intrusion. Two alternative processes may have controlled the rise of the silicate magma within the volcano conduit immediately after the termination of the diking event: (1) Increased buoyancy in the deep-seated chamber due to magma withdrawal and temporary pressure drop; (2) bubble rise and growth due to the passage of seismic waves from the earthquake swarm. Similar to the 2007 event, previous major ash eruptions at Oldoinyo Lengai volcano in the past half century were also preceded by earthquake swarms. Based on the large dike-related moment produced in the 2007 event, we expect future body wave inversions of its seismic part to show significant non-double couple moment tensor components.

Acknowledgements

This study was carried out within the framework of ESA AO ALOS-ADEN, project 3580. We thank the European Space agency for providing the SAR data and for their quick response in programming unscheduled acquisitions along with the development of events. An early version of the manuscript benefited from constructive comments made by M. Abelson, R. Amit, Z.B. Begin, A. Salamon and A. Ziv. Fruitful discussions with N. Lensky and V. Lyakhovsky are highly appreciated. Our warm thanks to A.M. Songo, University of Dar es-Salaam, for organizing the October field trip to Mt. Gelai, and to R.W. Ferdinand for productive discussions and for facilitating the contacts with the local field guides. Special thanks to Lesoiya Lerwaha and Sangau Alaigwanan, as well as to numerous Massai residents, who provided most friendly and very useful guidance and account of events. We thank the editor, Claude Jaupart and three anonymous reviewers for their thorough reviews which improved this paper significantly.

Appendix A. Supplementary data

Supplementary data associated with this article can be found, in the online version, at doi:10.1016/j.epsl.2008.04.052.

References

Aoki, Y., Segall, P., Kato, T., Cervelli, P., Shimada, S., 1999. Imaging magma transport during the 1997 seismic swarm off the Izu Peninsula, Japan. Science 286, 927–930.
Baker, B.H., Mohr, P.A., Williams, L.A.J., 1972. Geology of the eastern rift system of Africa. Geol. Soc. Am. Spec. Pap. 136, 1–67.
Benoit, J.P., McNutt, S.R., 1996. Global volcanic earthquake swarm database 1979–1989. U.S. Geological Survey Open File Report USGS OFR96-39. 333 pp.
Calais, E., Ebinger, C.J., Hartnady, C., Nocquet, J.M., 2006. Kinematics of the East African rift from GPS and earthquake slip vector data. In: Yirgu, G., Ebinger, C.J., Maguire, P.K.H. (Eds.), The Afar Volcanic Province Within the East African Rift System. Geological Society Special Publication, vol. 259, pp. 9–22.
Dawson, J.B., 1962. Sodium carbonate lavas from Oldoinyo Lengai, Tanganyika. Nature 195, 1075–1076.
Dawson, J.B., 1992. Neogene tectonics and volcanicity in the North Tanzania Sector of the Gregory Rift Valley: contrasts with the Kenya sector. Tectonophysics 204, 81–92.
Dawson, J.B., 1993. A supposed sövite from Oldoinyo Lengai, Tanzania: result of extreme alteration of alkali carbonate lava. Mineral. Mag. 57, 93–101.
Dawson, J.B., Keller, J., Nyamweru, C., 1995. Historic and recent eruptive activity of Oldoinyo Lengai. In: Bell, K., Keller, J. (Eds.), Carbonatite Volcanism. Springer-Verlag, pp. 4–22.
Dawson, J.B., Smith, J.V., Steele, I.M., 1992. 1966 ash eruption of the carbonatite volcano Oldoinyo Lengai: mineralogy of lapilii and mixing of silicate and carbonate magmas. Mineral. Mag. 56, 1–16.
Dawson, J.B., Pinkerton, H., Pyle, D.M., Nyamweru, C., 1994. June 1993 eruption of Oldoinyo Lengai, Tanzania: exceptionally viscous and large carbonatite flows and evidence for co-existing silicate and carbonate magmas. Geology 22, 799–802.
Einarsson, P., Brandsdottir, B., 1980. Seismological evidence for lateral magma intrusion during the July 1978 deflation of the Krafla volcano in NE-Iceland. J. Geophys. 47, 160–165.
EMSC catalog at: http://www.emsc-csem.org/index.php?page=home.
Fairhead, J.D., Girdler, R.W., 1971. The seismicity of Africa. Geophys. J. R. Astron. Soc. 24, 271–301.
Farr, T., Kobrick, M., 2000. Shuttle Radar Topography Mission produces a wealth of data. EOS, Trans. – Am. Geophys. Union 81, 583–585.
Fialko, Y., 2004. Probing the mechanical properties of seismically active crust with space geodesy: study of the co-seismic deformation due to the 1992 Mw 7.3 Landers (southern California) earthquake. J. Geophys. Res. 109, B03307.
Foster, A.N., Ebinger, C.J., Mbede, E., Rex, D., 1997. Tectonic development of the northern Tanzania sector of the East African Rift System. J. Geol. Soc. London 154, 689–700.
Gillard, D., Rubin, A.M., Okubo, P., 1996. Highly concentrated seismicity caused by deformation of Kilauea's deep magma system. Nature 384, 343–346.
Hamiel, Y., Fialko, Y., 2007. Structure and mechanical properties of faults in the North Anatolian Fault system from InSAR observations of coseismic deformation due to the 1999 Izmit (Turkey) earthquake. J. Geophys. Res. 112, B07412. doi:10.1029/2006JB004777.
Hill, D.P., 1977. A model for earthquake swarms. J. Geophys. Res. 82, 1347–1352.
Hill, D.P., Pollitz, F., Newhall, C., 2002. Earthquake–volcano interactions. Phys. Today 55, 41–47.
International Seismological Centre, On-line Bulletin, http://www.isc.ac.uk., International Seismological Centre, Thatcham, United Kingdom, 2001.
Jarvis, A., Reuter, H.I., Nelson, A., Guevara, E., 2006. Hole-filled SRTM for the Globe. Version 3, available from the CGIAR-CSI SRTM 90 m Database: http://srtm.csi.cgiar.org.
Jestin, F., Huchon, P., Gaulier, J.M., 1994. The Somalia plate and the East Africa Rift System. Geophys. J. Int. 116, 637–654.
Jónsson, S., Zebker, H., Segall, P., Amelung, F., 2002. Fault slip distribution of the 1999 Mw 7.1 Hector Mine earthquake, California, estimated from satellite radar and GPS measurements. Bull. Seismol. Soc. Am. 92 (4), 1377–1389.
Kanamori, H., 1977. The energy release in great earthquakes. J. Geophys. Res. 82, 2981–2987.
Kjarsgaard, B.A., Hamilton, D.L., 1989. The genesis of carbonatites by immiscibility. In: Bell, K. (Ed.), Carbonatites – genesis and evolution. Unwin Hyman, London, pp. 388–404.
Linde, A.T., Sacks, I.S., 1998. Triggering of volcanic eruptions. Nature 395, 888–890.
Linde, A.T., Sacks, I.S., Johnston, M.J.S., Hill, D.P., Bilham, R.G., 1994. Increased pressure from rising bubbles as a mechanism for remotely triggered seismicity. Nature 371, 408–410.
Lu, Z., Wicks Jr., C., Power, J.A., Dzurisin, D., 2000. Ground deformation associated with the March 1996 earthquake swarm in Akutan volcano, Alaska, revealed by satellite radar interferometry. J. Geophys. Res. 105, 21483–21495.
Lundgren, P., Stramondo, S., 2002. Slip distribution of the 1997 Umbria–Marche earthquake sequence: Joint inversion of GPS and synthetic aperture radar interferometry data. J. Geophys. Res. 107, 2316.
MacIntyre, R.M., Mitchell, J.G., Dawson, J.B., 1974. Age of fault movements in Tanzanian sector of East African Rift System. Nature 247, 354–356.
Manga, M., Brodsky, E., 2006. Seismic triggering of eruptions in the far field: volcanoes and geysers. Annu. Rev. Earth Planet. Sci. 34, 263–291.
Massonnet, D., Feigl, K.L., 1998. Radar interferometry and its applications to changes in the Earth's surface. Rev. Geophys. 36, 441–500.
McKenzie, D.P., Davis, D., Molnar, P., 1970. Plate tectonics of the Red Sea and East Africa. Nature 226, 243–248.
Mitchell, R.H., Dawson, J.B., 2007. The 24th September 2007 ash eruption of the carbonatite volcano Oldoinyo Lengai, Tanzania: mineralogy of the ash and implications for formation of a new hybrid magma type. Miner. Mag. 71, 483–492. doi:10.1180/minmag.2007.071.5.483.
Mogi, K., 1963. Some discussions on aftershocks, foreshocks, and earthquake swarms. Bull. Earthq. Res. Inst. Univ. Tokyo 41, 615–658.
Nakamura, H., 1975. Volcano structure and possible mechanical correlation between volcanic eruptions and earthquakes. Bull. Volcanol. Soc. Japan 2, 229–240.
Nyblade, A.A., Owens, T.J., Gurrola, H., Ritsema, J., Langston, C.A., 2000. Seismic evidence for a deep upper mantle thermal anomaly beneath East Africa. Geology 7, 599–602.
NEIC catalog at: http://neic.usgs.gov/neis/epic/epic_rect.html..

Okada, Y., 1985. Surface deformation due to shear and tensile faults in a half space. Bull. Seismol. Soc. Am. 75, 1135–1154.
Peterson, T.D., Kjarsgaard, B.A., 1995. What are the parental magmas at Oldoinyo Lengai? In: Bell, K., Keller, J. (Eds.), Carbonatite Volcanism. Springer-Verlag, pp. 148–162.
Petibon, C.M., Kjarsgaard, B.A., Jenner, G.A., Jackson, S.E., 1998. Phase relationships of a silicate-bearing natrocarbonatite from Oldoinyo Lengai at 20 and 100 MPa. J. Petrol. 39, 2137–2151.
Pollard, D.D., Delaney, P.T., Duffield, W.A., Endo, E.T., Okamura, A.T., 1983. Surface deformation in volcanic rift zones. Tectonophysics 94, 541–584.
Rosen, P.A., Henseley, S., Peltzer, G., Simons, M., 2004. Updated repeat orbit interferometry package released. EOS, Trans. – Am. Geophys. Union 85 (5), 35.
Rubin, A.M., Pollard, D.D., 1988. Dike-induced faulting in rift zones of Iceland and Afar. Geology 16, 413–417.
Scordilis, E.M., 2006. Empirical global relations converting Ms and mb to moment magnitude. J. Seismol. 10, 225–236.
Stamps, D.S., Calais, E., Saria, E., Hartnady, C., Nocquet, J.-M., Ebinger, C., Fernandes, R.M., 2008. A kinematic model for the East African Rift. Geophys. Res. Lett. 35, L05304. doi:10.1029/2007GL032781.
Stein, R.S., 2004. Tidal triggering caught in the act. Science 305, 1248–1249.
Sykes, L.R., 1970. Earthquake swarms and sea-floor spreading. J. Geophys. Res. 75, 6598–6611.
Toda, S., Stein, R.S., 2002. Response of the San Andreas Fault to the 1983 Coalinga–Nuñez Earthquakes: an application of interaction-based probabilities for Parkfield. J. Geophys. Res. 107. doi:10.1029/2001JB000172.
Toda, S., Stein, R.S., Sagiya, T., 2002. Evidence from the AD 2000 Izu islands earthquake swarm that stressing rate governs seismicity. Nature 419, 58–61.
Ukawa, M., Tsukahara, H., 1996. Earthquake swarms and dike intrusions off the east coast of Izu Peninsula, central Japan. Tectonophysics 253, 285–303.
Vidale, J.E., Boyle, K.L., Shearer, P.M., 2006. Crustal earthquake bursts in California and Japan: their patterns and relations to volcanoes. Geophys. Res. Lett. 33, L20313.
Walter, T.R., 2007. How a tectonic earthquake may wake up volcanoes: stress transfer during the 1996 earthquake-eruption sequence at the Karymsky Volcanic Group, Kamchatka. Earth Planet. Sci. Lett. 264, 347–359.
Walter, T.R., Amelung, F., 2006. Volcano-earthquake interaction at Mauna Loa volcano, Hawaii. J. Geophys. Res. 111, B05204. doi:10.1029/2005JB003861.
Werner, C., Wegmuller, U., Strozzi, T., Weismann, A., 2003. Interferometric Point Target Analysis for Deformation Mapping, Proceedings of IGARSS'03, Toulouse, France, 21-25 July.
Wright, T.J., Ebinger, C., Biggs, J., Ayele, A., Yirgu, G., Keir, D., Stork, A., 2006. Magma-maintained rift segmentation at continental rupture in the 2005 Afar dyking episode. Nature 442, 291–294.